Supporting information

Phenoxazine-based scaffold for designing G4-interacting agents

Vladimir B. Tsvetkov,[a,b,c] Anna M. Varizhuk,[a,d] Sofia A. Lizunova,[a,e] Tatiana A. Nikolenko,[a,e] Igor A. Ivanov,[f] Vjacheslav V. Severov,[a] Evgeny S. Belyaev,[g] Egor A. Shitikov,[a] Galina E. Pozmogova,*[a] and Andrey V. Aralov*[f]

1. Experimental section

1.1 Molecular Modeling

The 3D models of the ligands and the target were built using the molecular graphics software package Sybyl-X (Certara, USA). Partial charges on the ligands atoms were calculated according to the following scheme. First, in order to find the most minimal conformation, scanning of the conformational space of the ligands was performed applying a molecular-mechanical approach and a Monte Carlo method by using Molsoft ICM-Pro 3.8.6.[1] To calculate interatomic interactions, the force field mmff[2] was used at this stage. Further optimization of the conformation found at the first step for the purpose of searching the geometry with the lowest energy and calculating the electron density distribution were performed by DFT using the hybrid functional HSEH1PBE (referred to as HSE06 approach)[3] and 6-311G++2d,2p Pople basis sets. Then the Merz-Singh-Kollman scheme[4] was applied to the electron density distribution obtained for calculating the grid for the electrostatic potential fitting with the following parameters: (6/41=10) - the number of surfaces around the atoms and (6/42=17) - the density of test points on these surfaces. The RESP (Restrained ElectroStatic Potential) method[5] was applied to the fitting of the grid obtained in the previous step for calculation of the partial atomic charges. All quantum mechanics simulations were carried out using the Gaussian 09 program.[6] To create the quadruplex 3D-model, the structure from pdb 2o3m without the first nucleotide was used. The resulting structure was optimized using the Sybyl-X and Powell's method[7] with the following settings: parameters for intermolecular interactions and the values of partial charges were taken from the force field amber7ff99, non-bonded cut-off distance equal to 8 Å, effect of the medium was taken into account by a dielectric constant of 1, the number of iterations equal to 1000, the simplex method in an initial optimization, and 0.05 kcal mol^{-1} $Å^{-1}$ energy gradient convergence criterion. To define the most probable binding site of the ligands on the target surface, the procedure of the flexible ligand docking was performed using ICM-Pro 3.8.6. The quadruplex conformation remained invariable during the docking procedure. Before starting a docking procedure the structures of the target and the ligands were converted into an ICM object: according to the ICM method, the molecular models were described using internal coordinates as variables. The parameters needed for interatomic energy calculation and the partial charges for the atoms of the target were taken from the ECEPP/3.[8] The biased probability Monte Carlo (BPMC) minimization procedure[9] was used for the global energy optimization. Description of the binding energy scoring used in docking and BPMC procedure is reported by R. Abagyan and M. Totrov.[10] The conformations with the best value of the scoring function from the final conformational stack obtained from docking were used as starting conformations for the molecular dynamics calculations.

Molecular dynamics simulations (MD) were carried out using the Amber 18 suite of programs.[11] An influence of the solvent was estimated with the application of the water molecules model OPC3.[12] The simulation was performed by using periodical boundary conditions and a rectangular box. The buffer between the quadruplex-ligand complex and the periodic box wall was at least 10 Å. The parameters needed for the interatomic energy calculation were taken from the force fields OL15[13] for the quadruplex and from the gaff2 AMBER force field[14] for the ligands. The cation K^+ was added in the centre between the quadruplex quartets. For neutralizing of the negative charge, K^+ ions were also used. At the beginning of computing, the investigated systems were minimized by two steps. At the first stage, the location of the solvent molecules was optimized by using 1000 steps (500 steps of steepest descent followed by 500 steps of conjugate gradient), with the mobility of all the solute atoms being restrained with a force constant of 500 kcal mol^{-1} $Å^{-2}$. At the second stage, the optimization was carried out without any restriction using 2500 steps (1000 steps of steepest decent, 1500 steps of conjugate gradient). Then the gradual heating to 300 K during 20 ps was performed. To avoid wild fluctuations for the investigated systems at this stage, weak harmonic restrains were used with a force constant of 10 kcal mol^{-1} $Å^{-2}$ for all the atoms that weren't part of the solvent. The SHAKE[15] algorithm was applied to constrain bonds to hydrogen atoms, allowing to use 2 fs step. Scaling of nonbonded 1–4 van der Waals and electrostatic interactions were performed by the standard amber values. The cutoff distance for non-bonded interactions was equal to 10 Å and the long-range electrostatics were calculated using the particle mesh

Ewald method.[16] The MD simulations in the production phase were carried out using constant temperature (T = 300 K) and constant pressure (p = 1 atm) over 80 ns. To control the temperature, a Langevin thermostat was used with the collision frequency of 1 ps^{-1}. Energies of the quadruplex-ligand complex were estimated by using the GBSA approach. The binding energy was calculated as the sum of the electrostatic energies (E_q), Van der Waals energies (E_{VDW}), and the solvation energy. The solvation energy was calculated as the sum of the polar and non-polar contributions. The polar contribution (EGB) was computed using the Generalized Born (GB) method and the algorithm developed by Onufriev et al. for calculating the effective Born radii.[17] The non-polar contribution to the solvation energy (E_{surf}), which includes solute-solvent van der Waals interactions and the free energy of cavity formation in the solvent, was estimated from the solvent-accessible surface area (SASA).

1.2 Chemistry

All reagents were commercially available unless otherwise mentioned and used without further purification. All solvents were purchased from commercial sources. Thin layer chromatography (TLC) was performed on plates (Merck) precoated with silica gel (60 µm, F254) and visualized using UV light (254 and 365 nm). Column chromatography (CC) was performed on silica gel (0.040−0.063 mm, Merck, Germany). ^{1}H and ^{13}C NMR spectra were recorded on the Bruker Avance III 600 spectrometer at 600 and 151 MHz, respectively. Chemical shifts are reported in δ (ppm) units using residual 1H signals from deuterated solvents as references. The multiplicity are reported using the following abbreviations: s (singlet), d (doublet), t (triplet), m (multiplet), br (broad). The coupling constants (J) are given in Hz. ESI HR mass spectra were acquired on a Thermo Scientific LTQ Orbitrap hybrid instrument (Thermo Electron Corp., Bremen, Germany) in continuous flow direct sample infusion (positive ion mode).

1-(3-azidopropyl)-5-bromouracil **2**

The mixture of 1-(3-bromopropyl)-5-bromouracil **1**[18] (2.71 g, 8.70 mmol) and NaN_3 (0.68 g, 10.5 mmol) in DMF (20 mL) was stirred overnight at room temperature. Then, it was poured into water (30 mL) and the product was extracted with CH_2Cl_2 (3 × 20 mL). The organics were concentrated and co-evaporated with toluene (2 × 20 mL). The residue was purified by column chromatography on silica gel (0-2% MeOH in CH_2Cl_2) yielding **2** (2.12 g, 7.80 mmol, 89 %) as a off-white solid. ^{1}H NMR (600 MHz, DMSO-d_6): δ 11.71 (br s, 1H), 8.20 (s, 1H), 3.74 (t, J = 6.9 Hz, 2H), 3.39 (t, J = 6.7 Hz, 2H), 1.85 (dd, J = 6.7, J = 6.9 Hz, 2H). ^{13}C NMR (151 MHz, DMSO-d_6): δ 159.6, 150.3, 145.2, 94.6, 47.9, 45.6, 27.4. HRMS (ESI) m/z: calcd for $C_7H_9BrN_5O_2^+$ $[M+H]^+$: 273.9934; found 273.9939.

4-((5-(3-azidopropoxy)-2-hydroxyphenyl)-1-(3-azidopropyl)-5-bromocytosine **3**

To a suspension of 1,2,4-triazole (2.55 g, 36.9 mmol) in dry CH_3CN (80 mL) $POCl_3$ (0.75 mL, 8.20 mmol) was added at 0°C followed by the addition of cold triethylamine (8.61 mL, 61.5 mmol). The mixture was stirred for 30 min at 0°C and added to the solution of **2** (1.12 g, 4.10 mmol) in dry CH_3CN (10 mL). The mixture was stirred for 4 h and concentrated in vacuo. The residue was distributed between CH_2Cl_2 (100 mL) and saturated aqueous $NaHCO_3$ solution (100 mL). The organic layer was washed with water (2x100 mL), dried over Na_2SO_4, filtered and concentrated in vacuo to afford triazole intermediate as an orange solid (1.24 g). The residue was dissolved in CH_2Cl_2 (40 mL) and added to 4-(3-bromopropoxy)-2-aminophenol[19] (1.62 g, 6.60 mmol) followed by the addition of DIPEA (1.2 mL, 6.60 mmol). After stirring overnight at room temperature the organic layer was subsequently washed with 2% aqueous citric acid solution (30 mL), saturated aqueous $NaHCO_3$ solution (30 mL) and water (2 × 30 mL) and concentrated in vacuo. The foam obtained was dissolved in DMF (15 mL) and NaN_3 (0.4 g, 6.20 mmol) was added. After stirring overnight at room temperature, the mixture was poured into water (30 mL) and the product was extracted with CH_2Cl_2 (3 × 20 mL). The organics were concentrated and co-evaporated with toluene (2 × 20 mL). The residue was purified by column chromatography on silica gel (0-1% MeOH in CH_2Cl_2) yielding **3** (1.03 g, 2.21 mmol, 54 %) as brownish solid. ^{1}H NMR (600 MHz, DMSO-d_6): δ 9.83 (br s, 1H), 8.29 (s, 1H), 8.20 (br s, 1H), 8.04 (d, J = 3.0 Hz, 1H), 6.82 (d, J = 8.7 Hz, 1H), 6.59 (dd, J = 3.0 Hz, J = 8.7 Hz, 1H), 3.95 (t, J = 6.1 Hz, 2H), 3.80 (t, J = 7.0 Hz, 2H), 3.51 (t, J = 6.7 Hz, 2H), 3.40 (t, J = 6.7 Hz, 2H), 1.97 (dd, J = 6.1, J = 6.7 Hz, 2H), 1.90 (dd, J = 6.7, J = 7.0 Hz, 2H). ^{13}C NMR (151 MHz, DMSO-d_6): δ 156.8, 153.8, 151.0, 146.9, 141.1, 126.7, 114.8, 109.1, 108.5, 86.6, 64.9, 48.1, 47.7, 47.00, 28.1, 27.5. HRMS (ESI) m/z: calcd for $C_{16}H_{19}BrN_9O_3^+$ $[M+H]^+$: 464.0789; found 464.0790.

8-(3-azidopropoxy)-3-(3-azidopropyl)-1,3-diaza-2-oxophenoxazine **4**

The cytosine derivative **3** (1.01 g, 2.18 mmol) was dissolved in a mixture of absolute C_2H_5OH (30 mL) and TEA (5.8 mL) and refluxed under N_2 for 48 hours. After concentration in vacuo, the residue was purified by column chromatography on silica gel (0-2% MeOH in CH_2Cl_2) yielding **4** (0.27 g, 0.70 mmol, 32 %) as yellowish solid. ^{1}H NMR (600 MHz, DMSO-d_6): δ 10.39 (br s, 1H), 7.38 (br s, 1H), 6.71 (d, J = 8.6 Hz, 1H), 6.42-6.37 (m, 2H), 3.93 (t, J = 6.1 Hz, 2H), 3.64 (t, J = 6.9 Hz, 2H), 3.48 (t, J = 6.7 Hz, 2H), 3.38 (t, J = 6.7 Hz, 2H), 1.93 (dd, J = 6.1, J = 6.7 Hz, 2H), 1.84 (dd, J = 6.7, J = 6.9 Hz, 2H). ^{13}C NMR (151 MHz, DMSO-d_6):

δ 154.3, 153.5, 136.0, 126.5, 115.3, 108.1, 103.6, 64.9, 48.00, 47.6, 46.1, 28.00, 27.4. HRMS (ESI) m/z: calcd for $C_{16}H_{18}N_9O_3^+$ $[M+H]^+$: 384.1527; found 384.1532.

3-(3-azidopropyl)-1,3-diaza-2-oxophenoxazine **6**

To a suspension of 1,2,4-triazole (2.18 g, 31.5 mmol) in dry CH_3CN (70 mL) $POCl_3$ (0.64 mL, 7.0 mmol) was added at 0°C followed by the addition of cold triethylamine (7.35 mL, 52.5 mmol). The mixture was stirred for 30 min at 0°C and added to **2** (0.88 g, 3.5 mmol). The mixture was stirred for 4 h and concentrated in vacuo. The residue was distributed between CH_2Cl_2 (100 mL) and saturated aqueous $NaHCO_3$ solution (100 mL). The organic layer was washed with water (2x100 mL), dried over Na_2SO_4, filtered and concentrated in vacuo to afford triazole intermediate as an orange solid (0.95 g). The residue was dissolved in CH_2Cl_2 (35 mL) and added to 2-aminophenol (0.62 g, 5.6 mmol) followed by the addition of DIPEA (1.0 mL, 5.6 mmol). After stirring overnight at room temperature, the organic layer was subsequently washed with 2% aqueous citric acid solution (30 mL), saturated aqueous $NaHCO_3$ solution (30 mL) and water (2 × 30 mL) and concentrated in vacuo. The foam obtained was dissolved in a mixture of absolute C_2H_5OH (25 mL) and TEA (4.9 mL) and refluxed under N_2 for 48 hours. After concentration in vacuo, the residue was purified by column chromatography on silica gel (0-2% MeOH in CH_2Cl_2) yielding **6** (0.19 g, 0.67 mmol, 19 %) as light brown solid. ^{1}H NMR (600 MHz, DMSO-d_6): δ 10.41 (br s, 1H), 7.39 (s, 1H), 6.88-6.81 (m, 2H), 6.80-6.76 (m, 2H), 3.65 (t, J = 6.9 Hz, 2H), 3.38 (t, J = 6.7 Hz, 2H), 1.84 (dd, J = 6.7, J = 6.9 Hz, 2H). ^{13}C NMR (151 MHz, DMSO-d_6): δ 153.5, 153.2, 142.1, 127.8, 126.6, 126.4, 123.5, 123.4, 116.7, 114.9, 48.00, 46.1, 27.4. HRMS (ESI) m/z: calcd for $C_{13}H_{13}N_6O_2^+$ $[M+H]^+$: 285.1095; found 285.1098.

10-(2-((2-aminoethyl)amino)-2-oxoethyl)-3-(3-azidopropyl)-1,3-diaza-2-oxophenoxazine **8**

To a solution of **6** (0.13 g, 0,46 mmol) in CH_2Cl_2 (5 mL) DBU (0.15 mL, 1.00 mmol) was added at room temperature. Then, methyl 2-bromoacetate (0.88 mL, 0.92 mmol) was added in one portion and the resulting mixture was stirred at room temperature for 1 hour and then poured into 5% aqueous citric acid solution (10 ml). The organics were extracted with CH_2Cl_2 (2 × 15 mL), dried over Na_2SO_4, filtered and concentrated in vacuo. The foam obtained was dissolved in MeOH (10 mL) and ethane-1,2-diamine (0.3 mL, 4.6 mmol) was added. The solution was heated at 50°C for 48 hours, concentrated and co-evaporated with toluene (2 × 10 mL) in vacuo. The residue was purified by column chromatography on silica gel (0-5% MeOH in CH_2Cl_2) yielding **8** (0.13 g, 0.34 mmol, 73 %) as light brown solid. ^{1}H NMR (600 MHz, DMSO-d_6): δ 7.55 (br t, 1H), 7.55 (s, 1H), 6.95-6.90 (m, 2H), 6.86-6.83 (m, 1H), 6.80-6.76 (m, 1H), 4.57 (s, 2H), 3.71 (t, J = 7.0 Hz, 2H), 3.39 (t, J = 6.8 Hz, 2H), 3.14-3.08 (m, 2H), 2.61 (t, J = 6.2 Hz, 2H), 1.84 (dd, J = 7.0, J = 6.8 Hz, 2H). ^{13}C NMR (151 MHz, DMSO-d_6): δ 166.1, 153.3, 153.3, 142.4, 127.9, 127.8, 126.3, 123.6, 123.1, 115.00, 114.4, 47.9, 46.2, 43.5, 41.9, 40.8, 27.3. HRMS (ESI) m/z: calcd for $C_{17}H_{21}N_8O_3^+$ $[M+H]^+$: 385.1731; found 385.1737.

General procedure for catalytic hydrogenation

A suspension of the corresponding azide (1 eq.) and 10% Pd/C (30 mg/mmol) in MeOH (5 mL/mmol) was stirred for 3 hours under hydrogen atmosphere. The catalyst was filtered off and the solution was concentrated under reduced pressure. The residue was triturated with CH_3CN yielding the corresponding amine:

8-(3-aminopropoxy)-3-(3-aminopropyl)-1,3-diaza-2-oxophenoxazine **5^{pro}**

This compound (190 mg, 0.57 mmol, 84 %) was prepared starting from **4** as yellowish solid. ^{1}H NMR (600 MHz, DMSO-d_6): δ 7.40 (s, 1H), 6.70 (d, J = 8.3 Hz, 1H), 6.41-6.35 (m, 2H), 3.92 (t, J = 6.0 Hz, 2H), 3.65 (t, J = 6.5, 2H), 2.72 (t, J = 6.2 Hz, 2H), 2.57 (t, J = 6.6 Hz, 2H), 1.82-1.75 (m, 2H), 1.72-1.66 (m, 2H). ^{13}C NMR (151 MHz, DMSO-d_6): δ 154.4, 153.3, 135.9, 128.4, 126.4, 126.2, 126.2, 115.0, 108.1, 103.6, 65.5, 45.7, 37.4, 37.4, 30.5, 30.2. HRMS (ESI) m/z: calcd for $C_{16}H_{22}N_5O_3^+$ $[M+H]^+$: 332.1717; found 332.1722.

3-(3-aminopropyl)-1,3-diaza-2-oxophenoxazine **7**

This compound (41 mg, 0,16 mmol, 78 %) was prepared starting from **6** as beige solid. ^{1}H NMR (600 MHz, DMSO-d_6): δ 7.42 (s, 1H), 6.87-6.80 (m, 2H), 6.80-6.74 (m, 2H), 3.64 (t, J = 6.8 Hz, 2H), 2.56 (t, J = 6.7 Hz, 2H), 1.68 (dd, J = 6.7, J = 6.8 Hz, 2H). ^{13}C NMR (151 MHz, DMSO-d_6): δ 153.5, 153.5, 142.1, 127.8,

126.7, 126.3, 123.4, 116.7, 114.9, 45.9, 37.7, 30.9. HRMS (ESI) m/z: calcd for $C_{13}H_{15}N_4O_2^+$ $[M+H]^+$: 259.1190; found 259.1193.

10-(2-((2-aminoethyl)amino)-2-oxoethyl)-3-(3-aminopropyl)-1,3-diaza-2-oxophenoxazine **9**

This compound (93 mg, 0.26 mmol, 80 %) was prepared starting from **8** as beige solid. ^{1}H NMR (600 MHz, DMSO-d_6): δ 8.36 (t, J = 5.2 Hz, 1H), 7.66 (s, 1H), 6.96-6.89 (m, 2H), 6.87-6.83 (m, 1H), 6.83-6.79 (m, 1H), 4.58 (s, 2H), 3.72 (t, J = 6.6 Hz, 2H), 3.19-3.13 (m, 2H), 2.69-2.63 (m, 4H), 1.81 (dd, J = 6.8, J = 6.6 Hz, 2H). ^{13}C NMR (151 MHz, DMSO-d_6): δ 166.3, 153.6, 153.3, 142.4, 127.9, 127.9, 126.4, 123.7, 123.2, 115.00, 114.5, 45.8, 43.5, 40.4, 40.1, 36.9, 28.8. HRMS (ESI) m/z: calcd for $C_{17}H_{23}N_6O_3^+$ $[M+H]^+$: 359.1826; found 359.1833.

1.3 FRET melting experiments

Oligonucleotides (ODNs) labeled with 6-carboxyfluorescein (FAM) and Blackhole quencher 1 (BHQ) residues (for FRET-melting assays), as well as the unlabeled ODN Hair (for the selectivity assay), were purchased from Litekh, Russia (purity > 95%, HPLC). Secondary structures of the labeled ODNs were verified by circular dichroism (CD) spectroscopy. The ODN solutions (3.5 μM) in a 20 mM sodium-phosphate buffer, pH 7.4 (for G4s) or 5.8 (for i-motifs), supplemented with 10 mM KCl (buffer 1) were heated to 95ºC and snap-cooled on ice to facilitate intramolecular folding prior to all measurements. CD spectra were recorded using a Chirascan spectrophotometer (Applied Photophysics) at 15ºC.

FRET-melting experiments were performed using preannealed 0,5 μM ODN solutions or 1:20 ODN-ligand mixtures in buffer1 (ligand concentration was 10 μM). Melting curves were obtained with a QuantStudio 5 PCR System (Thermo Fisher Scientific). Fluorescence changes at 520 nm were recorded every 0.3ºC upon step-hold heating of the samples at an average rate of 1.5 ºC/min. Melting temperatures were determined from the maxima of the first derivatives of the melting curves.

For the selectivity assay, buffer conditions were altered in the case of cMyc to adjust its thermal stability in the absence of the ligands. cMyc was dissolved in buffer 2 (5 mM sodium-phosphate buffer, pH 7.4, 0.1 mM KCl, and 25 mM LiCl), and other labeled ODNs were dissolved in buffer 1. The labeled G4 ODNs were mixed with the preannealed unlabeled hairpin HAIR (G4 and hairpin concentrations: 0.5 μM and 10 μM, respectively); then, the ligand was added to a final concentration of 10 μM, and all melting experiments were repeated.

For the concentration-dependence assay, FRET-melting experiments were repeated with 1:1, 1:2, 1:5, and 1:10, and 1:20 ODN: ligand mixtures in buffer 1 (ODN concentration was 1 μM). The control ligand pyridostatin was purchased from Sigma-Aldrich.

1.4 Microscale thermophoresis (MST) assay

The preannealed 100 nM solution of HEX-22AG (HEX-AGGGTTAGGGTTAGGGTTAGGG) in buffer 1 (20 mM sodium-phosphate buffer, pH 7.4, and 10 mM KCl) was mixed 1:1 with 0-20 μM ligand solutions in buffer 1 supplemented with 5% DMSO, and the mixtures were stored at room temperature for 10 min prior to MST measurements. MST curves were registered using Monolith NT.115 and standard capillaries (NanoTemper, Germany) at 22 °C with MST monitoring by HEX fluorescence in a GREEN mode. The dependence of the normalized HEX fluorescence after termodiffusion on ligand concentration was analyzed using MO.Affinity Analysis software (NanoTemper, Germany). To obtain dissociation constant values, experimental data were fitted to the Hill model.

2. Supplementary figures

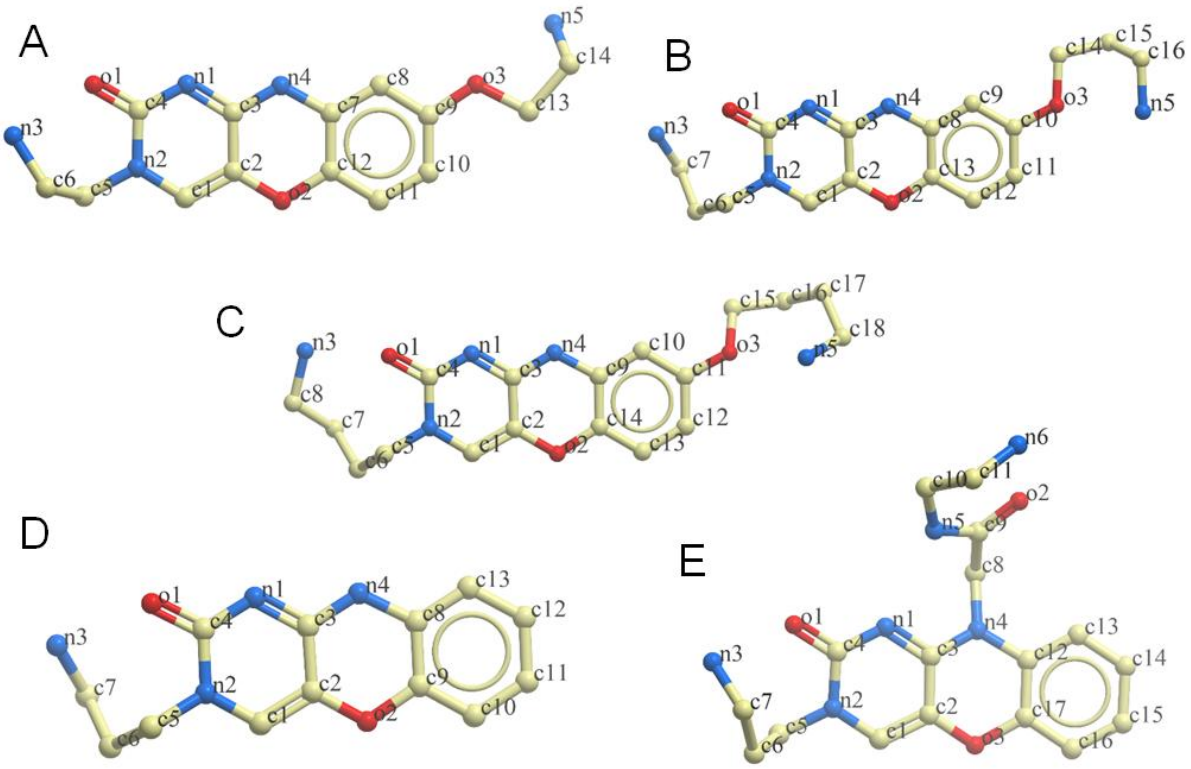

Figure S1. Structures of the ligands, obtained after quantum mechanical optimization: A – **5**^{et}, B – **5**^{pro}, C – **5**^{but}, D – **7**, E – **9**. Atoms are represented by the following colours: carbon – yellow, oxygen – red, nitrogen – blue. Hydrogens are not shown.

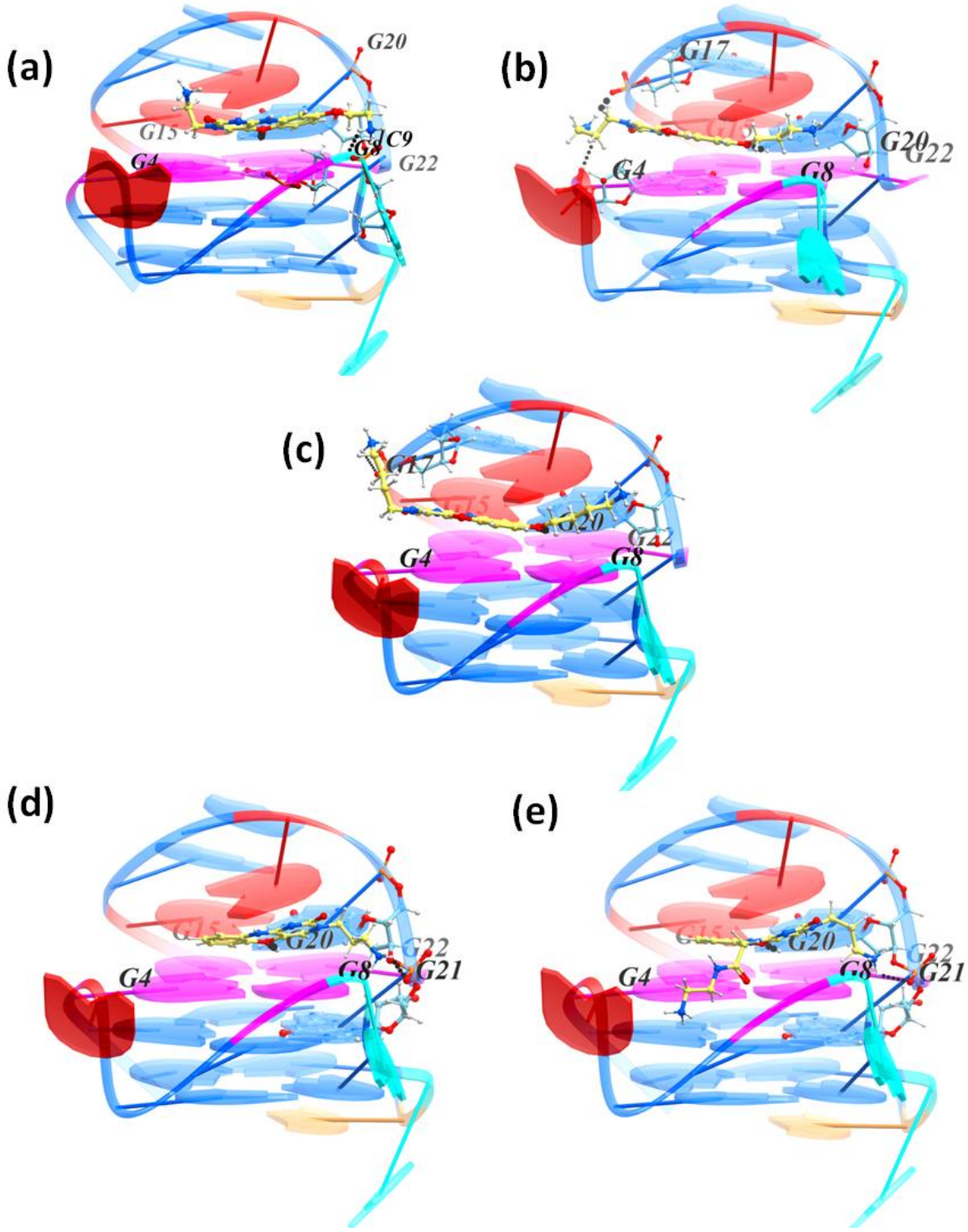

Figure S2. The lowest energy complex structures obtained by docking to c-Kit G4: a – **5**$^{\mathbf{et}}$, b – **5**$^{\mathbf{pro}}$, c – **5**$^{\mathbf{but}}$, d – **7**, e - **9**. The DNA shown by rendering with the nucleotides colored as follows: G in $G^4G^8G^{15}G^{22}$ tetrad – magenta, other G – blue, A – red, T – light brown. Nucleotides forming hydrogen bonds with the ligands are highlighted by rendering. Atoms are represented by the following colours: ligand carbon – yellow, DNA carbon – cyan, oxygen – red, nitrogen – blue, and hydrogen – white. Hydrogen bonds are shown as dashed lines; the thickness depends on the binding energy.

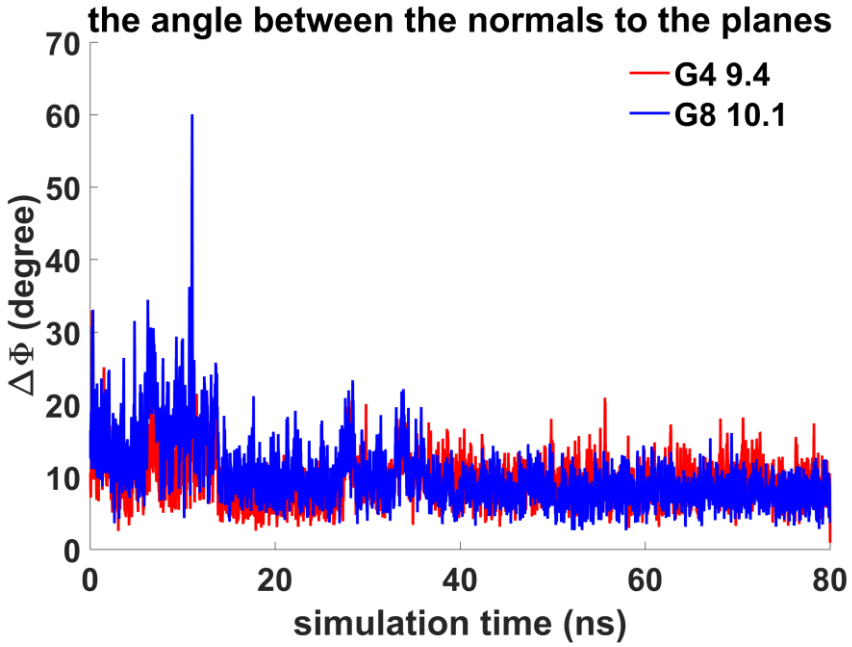

Figure S3. Evolution of the angle value between the normals to the plane of phenoxazine moiety of $\mathbf{5^{pro}}$ and the base planes of the nucleotides G4 and G8.

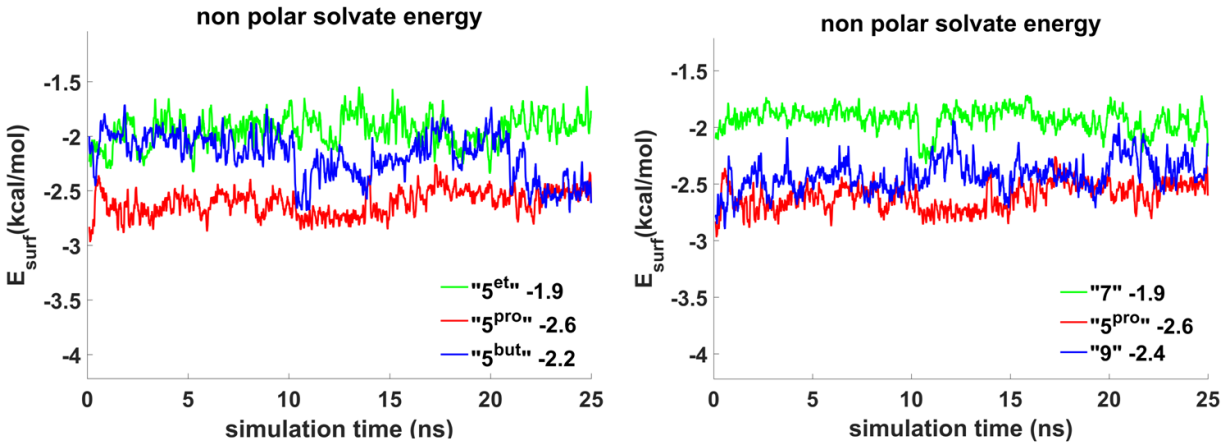

Figure S4. Evolution of the contribution of the nonpolar solvation energy component to the binding energy. The plots were smoothed using the moving average method (span = 5). Average values are indicated in figure legends.

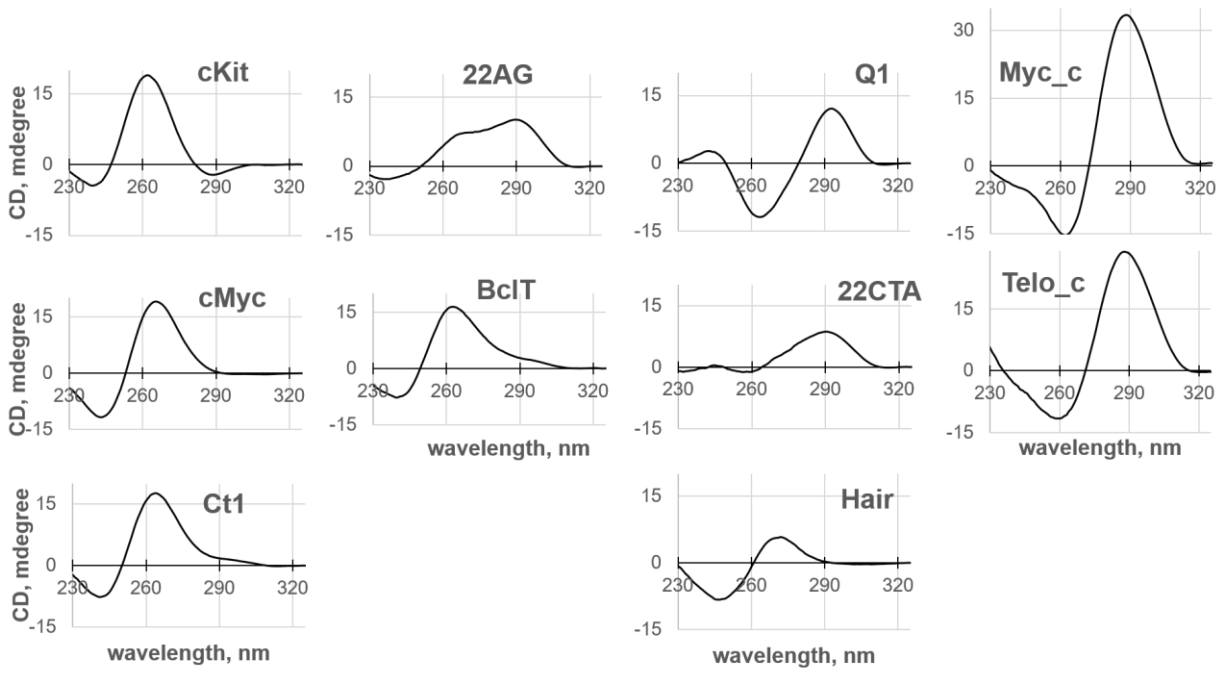

Figure S5. CD spectra of the FAM/BHQ-labeled ODNs. ODN concentration: 3,5 µM ODN; buffer conditions: 20 mM sodium-phosphate, pH 7.4 (for ODNs cKit, cMyc, Ct1, 22AG BclT, Q1, 22CTA and Hair) or 5.8 (for Myc_c and Telo_c), and 10 mM KCl; temperature: 15ºC.

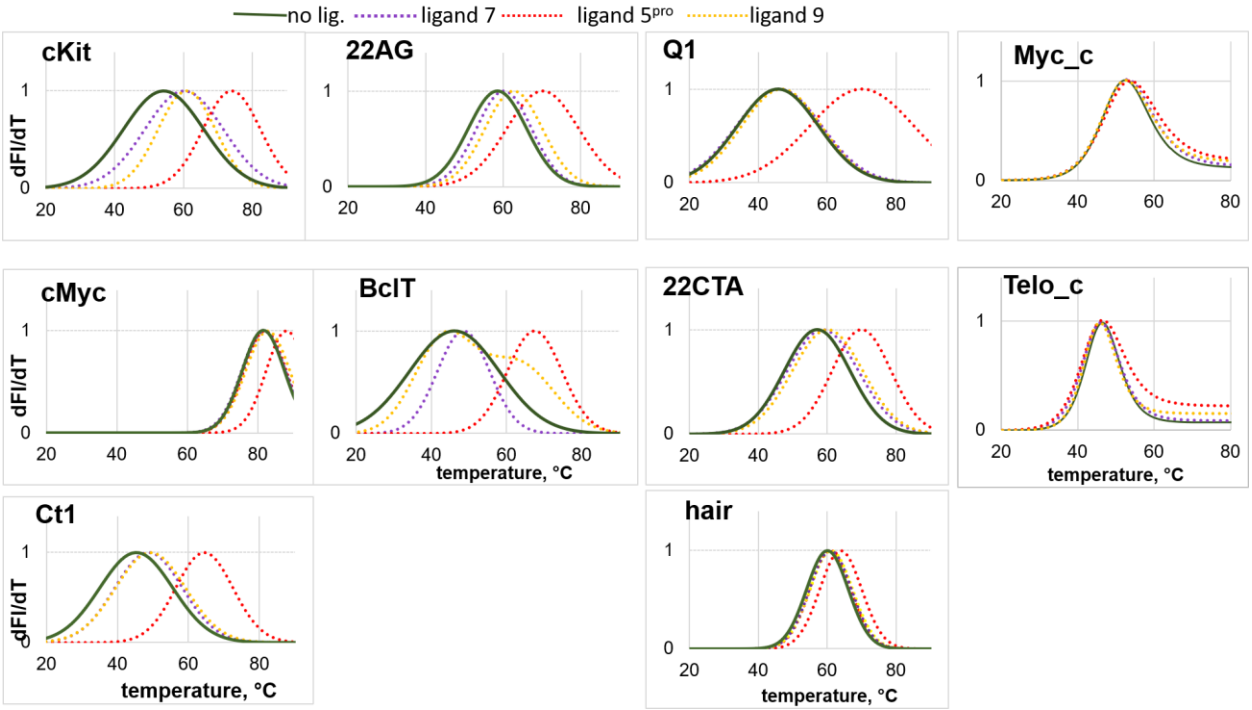

Figure S6. Melting curves of the labeled ODNs in the presence of the new ligands at a fixed concentration. Conditions: 20 mM sodium-phosphate buffer, pH 7.4 (for ODNs cKit, cMyc, Ct1, 22AG BclT, Q1, 22CTA and Hair) or 5.8 (for Myc_c and Telo_c), and 10 mM KCl. ODN concentration: 0.5 µM; ligand concentration: 10 µM.

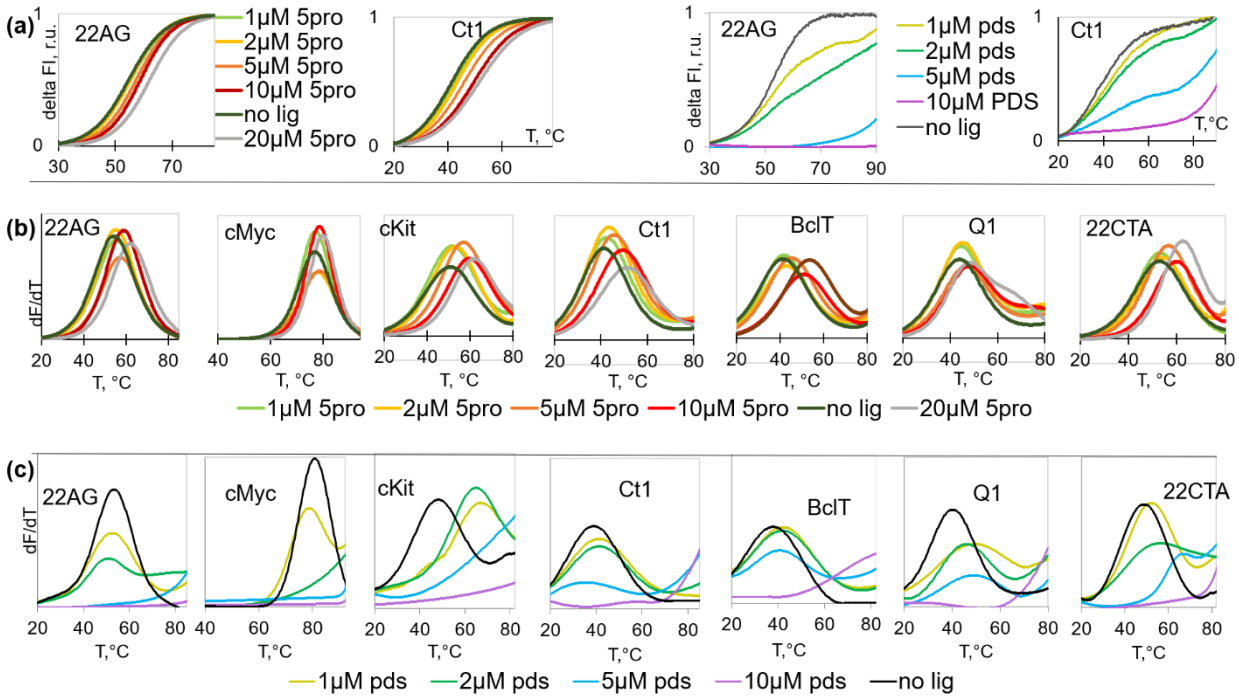

Figure S7. Melting curves of the labeled ODNs in the presence of $\mathbf{5}^{\mathbf{pro}}$ or **PDS**: concentration dependence analysis. (a) Representative melting curves obtained in the presence of 1-20 µM $\mathbf{5}^{\mathbf{pro}}$ (left) and 1-10 µM **PDS** (right). (b) First derivatives of the melting curves obtained with $\mathbf{5}^{\mathbf{pro}}$. (c) First derivatives of the melting curves obtained with **PDS**. Conditions: 20 mM sodium-phosphate buffer, pH 7.4 and 10 mM KCl. ODN concentration: 1 µM.

3. Supplementary tables

Table S1. Percentage of snapshots with H-bonds from MD simulations.

Ligand	donor	acceptor	occupancy
7	**7**-N3	DC9-OP1	29.43%
	7-N3	DG21-OP2	34.19%
	7-N3	DG8-O3'	7.32%
	DG20-N2	**7**-O2	12.83%
	7-N3	DG21-OP1	0.04%
	7-N3	DG20-O3'	0.12%
5^{et}	**5^{et}**-N3	DG18-OP2	8.44%
	5^{et}-N5	DG21-OP2	9.56%
	DG20-N2	**5^{et}**-O2	1.04%
	5^{et}-N3	DG17-O3'	0.24%
	5^{et}-N5	DG21-OP1	0.04%
	5^{et}-N5	DC9-OP1	11.48%
	5^{et}-N5	DG8-O3'	2.68%
	5^{et}-N3	DA19-N1	0.04%
	5^{et}-N5	DG20-O3'	0.04%
5^{pro}	**5^{pro}**-N3	DG17-OP2	11.48%
	5^{pro}-N3	DG4-OP1	19.63%
	5^{pro}-N5	DA19-O4'	0.20%
	5^{pro} -N5	DG20-O4'	0.40%
	DG20-N2	**5^{pro}**-O3	6.08%
	5^{pro}-N5	DA19-O3'	0.24%
	5^{pro}-N4	DG15-O6	0.04%
	5^{pro}-N5	DG20-OP2	0.04%
	5^{pro}-N4	DA16-N3	24.59%
	5^{pro}-N5	DA19-N3	0.12%
	5^{pro}-N3	DG4-OP2	0.16%
5^{but}	DG20-N2	**5^{but}**-O3	49.98%
	5^{but}-N5	DG20-OP2	14.15%
	5^{but}-N5	DG20-O5'	5.84%
	5^{but}-N3	DG18-OP2	0.16%
	5^{but}-N3	DG17-OP2	0.44%
	5^{but}-N5	DA19-O3'	0.44%
	5^{but}-N3	DA5-OP1	10.64%
	5^{but}-N3	DA5-OP2	0.08%
	5^{but}-N5	DA19-O4'	0.40%
	5^{but}-N5	DA19-N3	2.08%
	5^{but}-N5	DA19-O5'	0.64%
	5^{but}-N5	DA19-OP2	0.52%
	5^{but}-N3	DG4-O3'	0.08%
	5^{but}-N5	DC9-OP1	3.08%
	5^{but}-N5	DG21-OP1	0.04%
	5^{but}-N5	DG8-O3'	0.20%
	5^{but}-N5	DG21-OP2	0.92%
9	**9**-N6	DG7-OP1	0.68%
	9-N3	DG8-O3'	3.20%
	9-N3	DG21-OP2	18.99%
	DG20-N2	**9**-O3	10.92%
	9-N3	DG21-OP1	0.28%
	9-N3	DC9-OP1	37.58%
	9-N6	DG8-OP1	10.16%
	9-N6	DG8-O5'	0.40%
	9-N3	DG20-O3'	0.24%
	9-N6	DG7-O3'	0.20%
	9-N6	DG8-OP2	0.36%

Table S2. ODN sequences and secondary structures.

code	folding type*	sequence
22AG	h-G4	FAM-AGGGTTAGGGTTAGGGTTAGGG-BHQ
cMyc	p-G4	FAM-TGAGGGTGGGTAGGGTGGGTAA-BHQ
c-Kit	p-G4	FAM-GGGAGGGCGCTGGGAGGAGGG-BHQ
Ct1	p-imG4	FAM-GGTGACAGGGGTATGGGGAGGGG-BHQ
BclT	p/h-imG4	FAM-GGGGACTTTCCAGGGAGGCGTGGCCTGGGCGGG-BHQ
Q1	a-G4	FAM-GGTTAGGTTAGGTTAGG-BHQ
22CTA	a/h-G4	FAM-AGGGCTAGGGCTAGGGCTAGGG-BHQ
Hair	hairpin	FAM-GTATAGCTATTTTTATAGCTATA-BHQ
Myc_c	i-motif	FAM-CCCCACCCTCCCCACCCTCCC-BHQ
Telo_c	i-motif	FAM-CCCAATCCCAATCCCAATCCC-BHQ

*h-G4, hybrid G4; p-G4, parallel G4; a-G4, antiparallel G4; imG4, imperfect G4.

4. NMR Spectra

1-(3-azidopropyl)-5-bromouracil **2**
1H spectrum

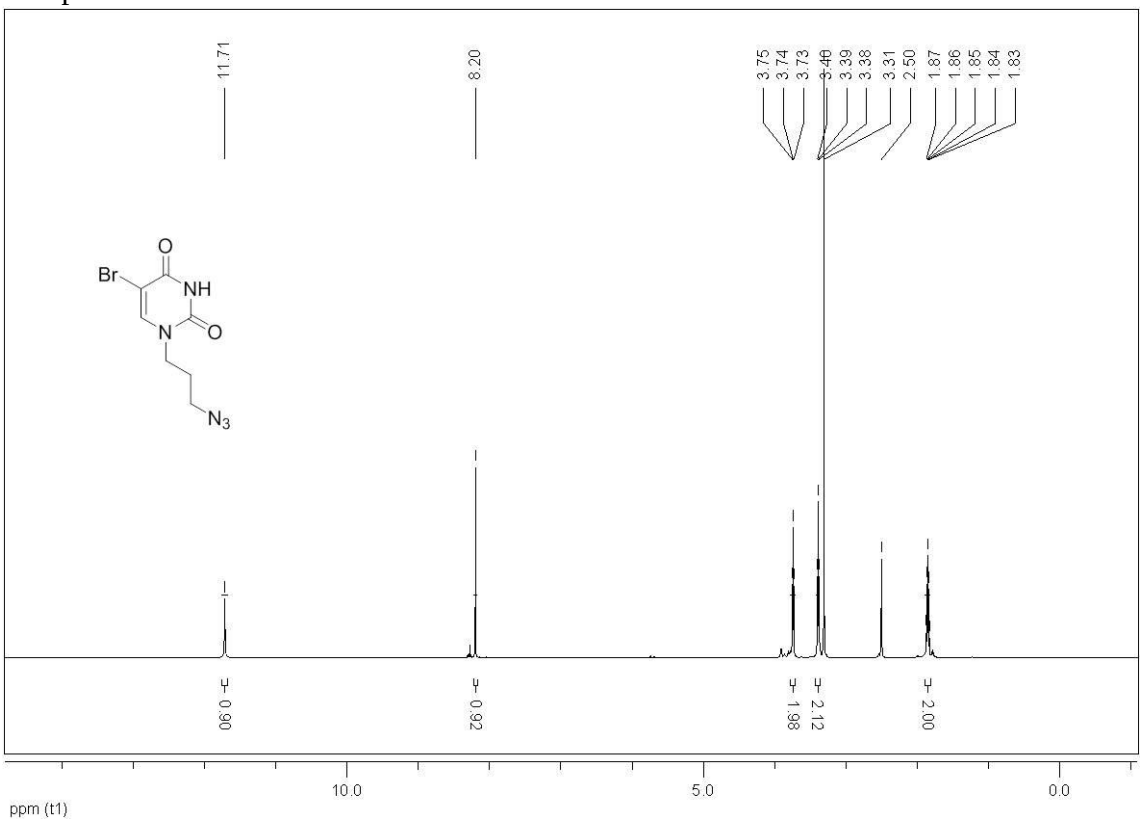

13C spectrum

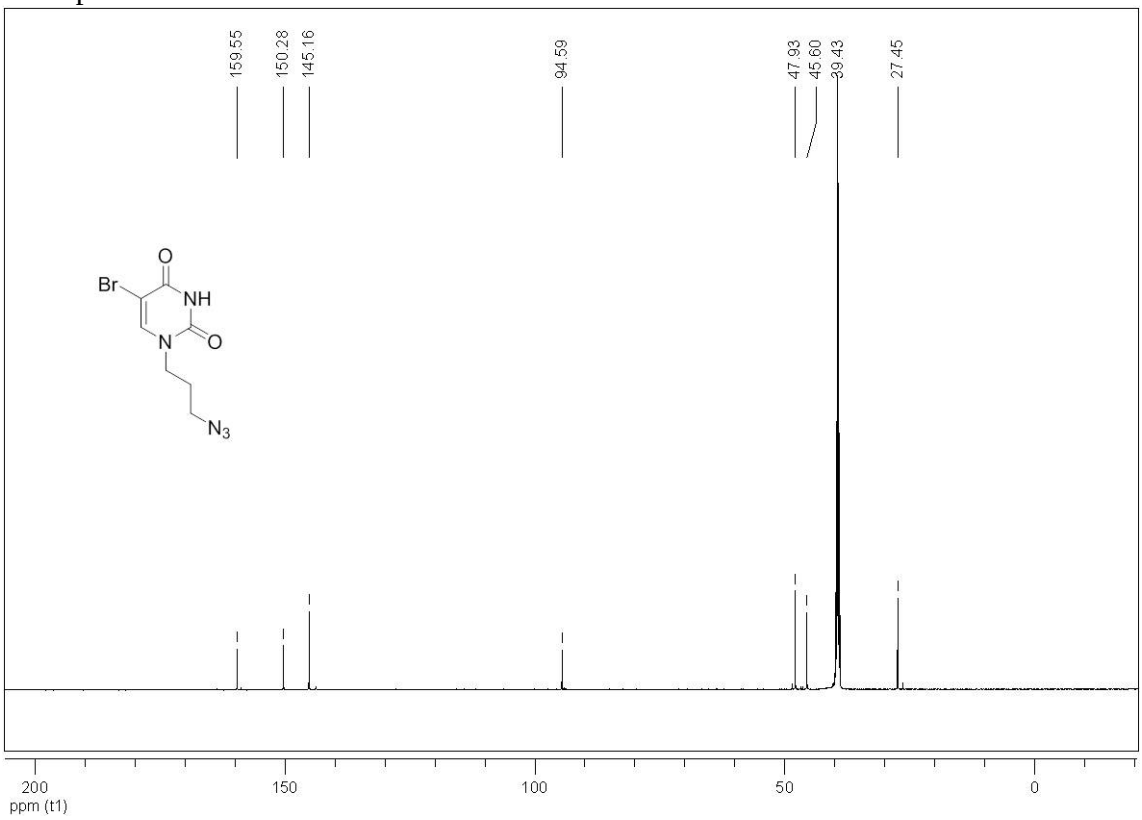

4-((5-(3-azidopropoxy)-2-hydroxyphenyl)-1-(3-azidopropyl)-5-bromocytosine **3**

1H spectrum

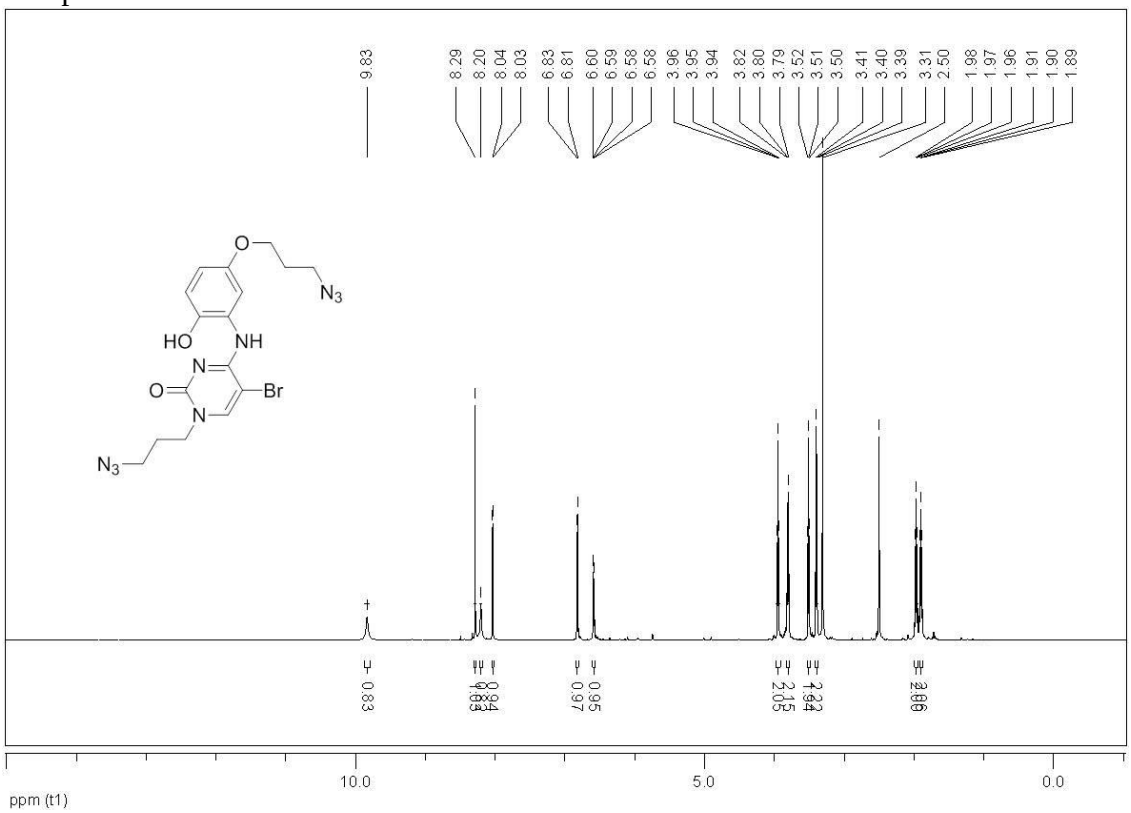

13C spectrum

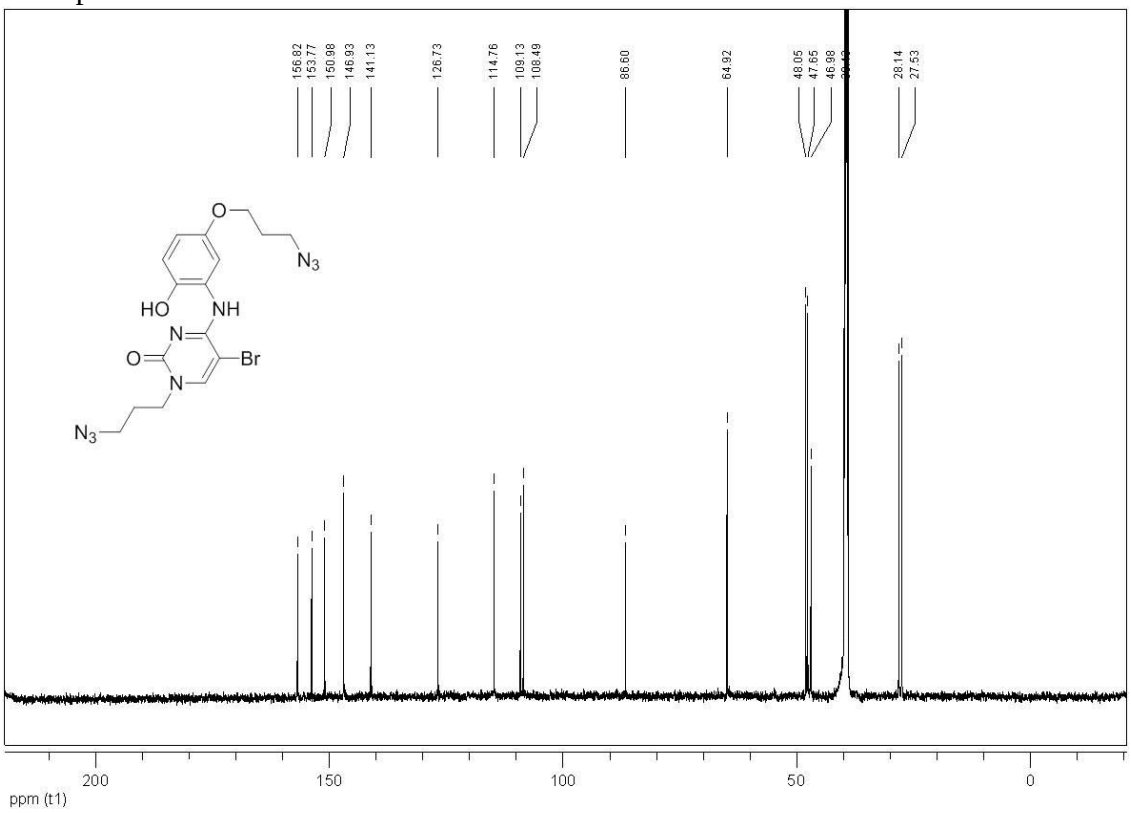

8-(3-azidopropoxy)-3-(3-azidopropyl)-1,3-diaza-2-oxophenoxazine **4**

1H spectrum

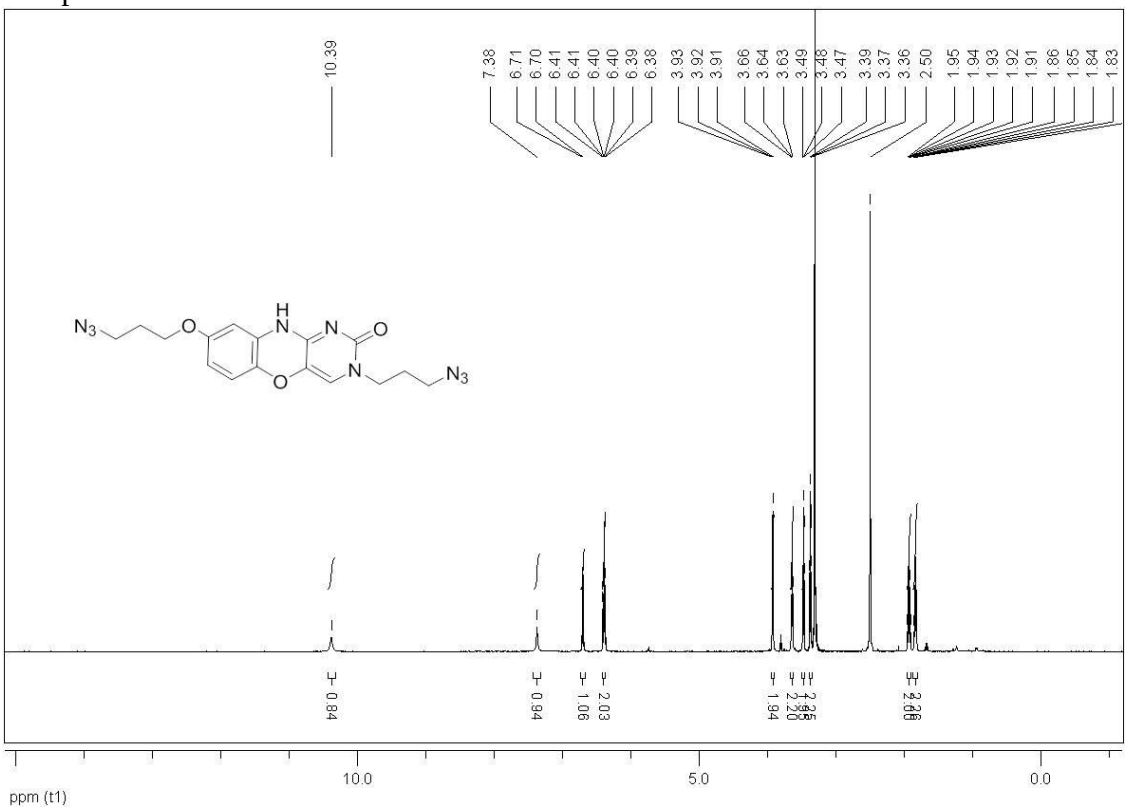

13C spectrum

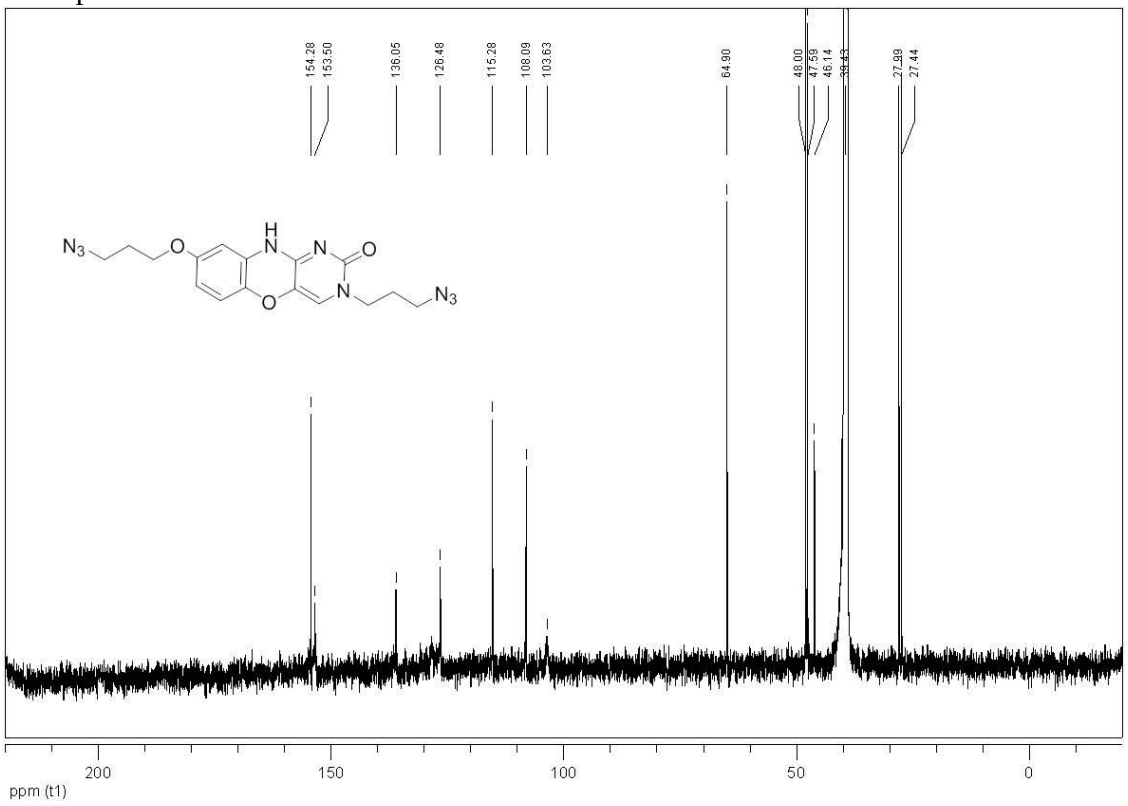

3-(3-azidopropyl)-1,3-diaza-2-oxophenoxazine **6**

1H spectrum

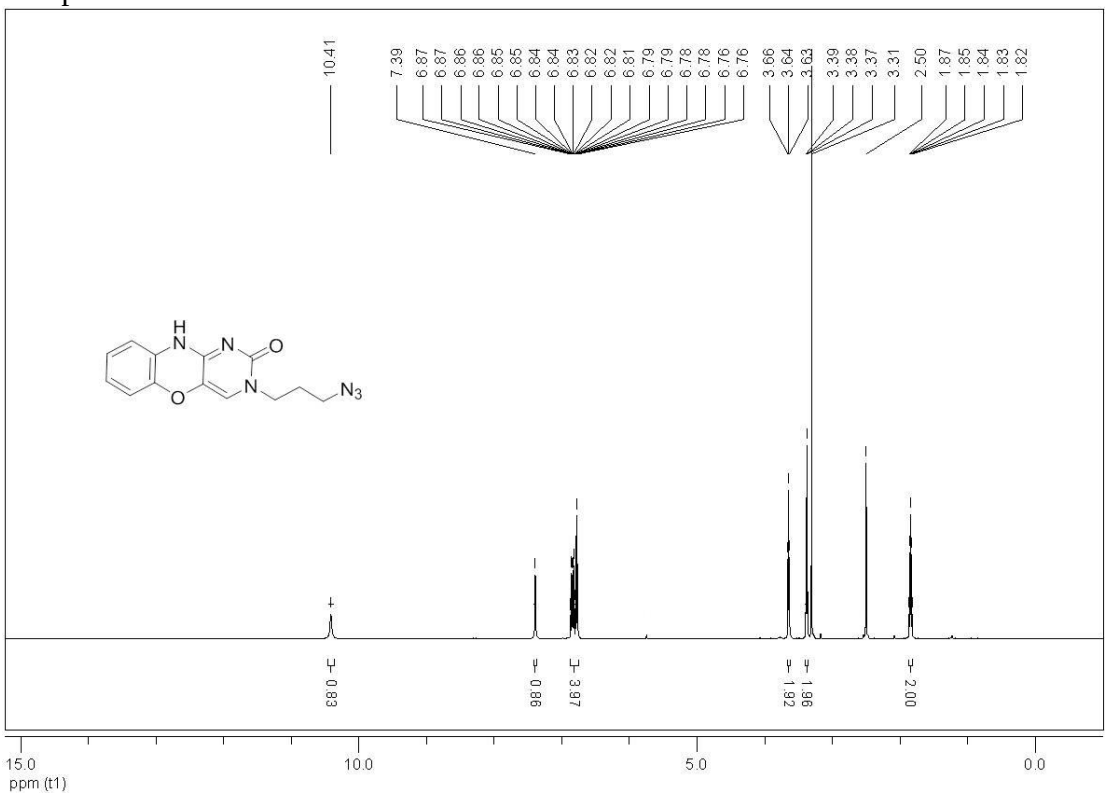

13C spectrum

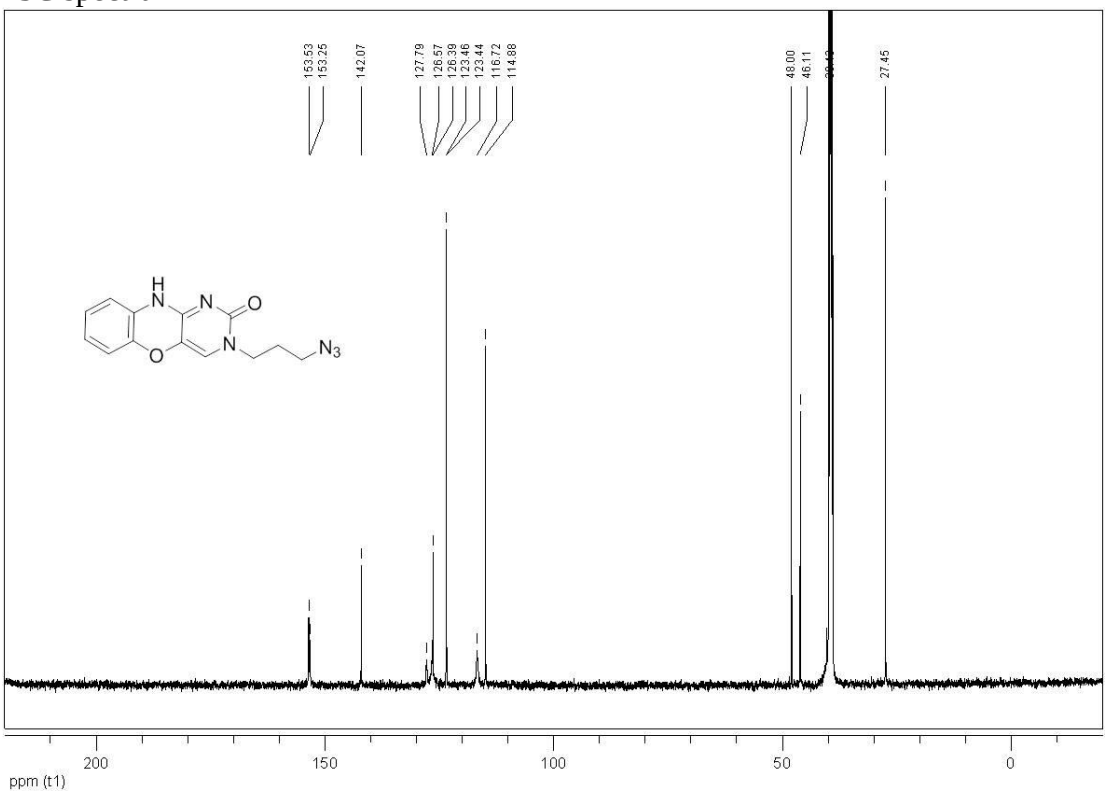

10-(2-((2-aminoethyl)amino)-2-oxoethyl)-3-(3-azidopropyl)-1,3-diaza-2-oxophenoxazine **8**

1H spectrum

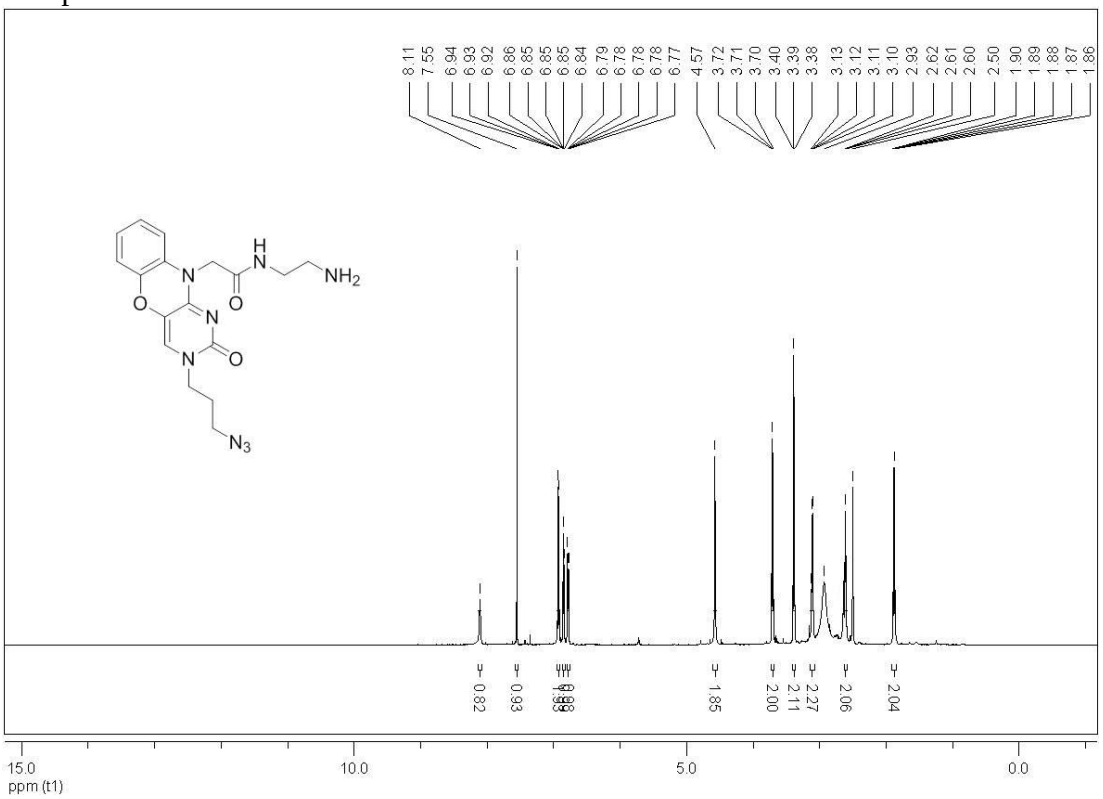

13C spectrum

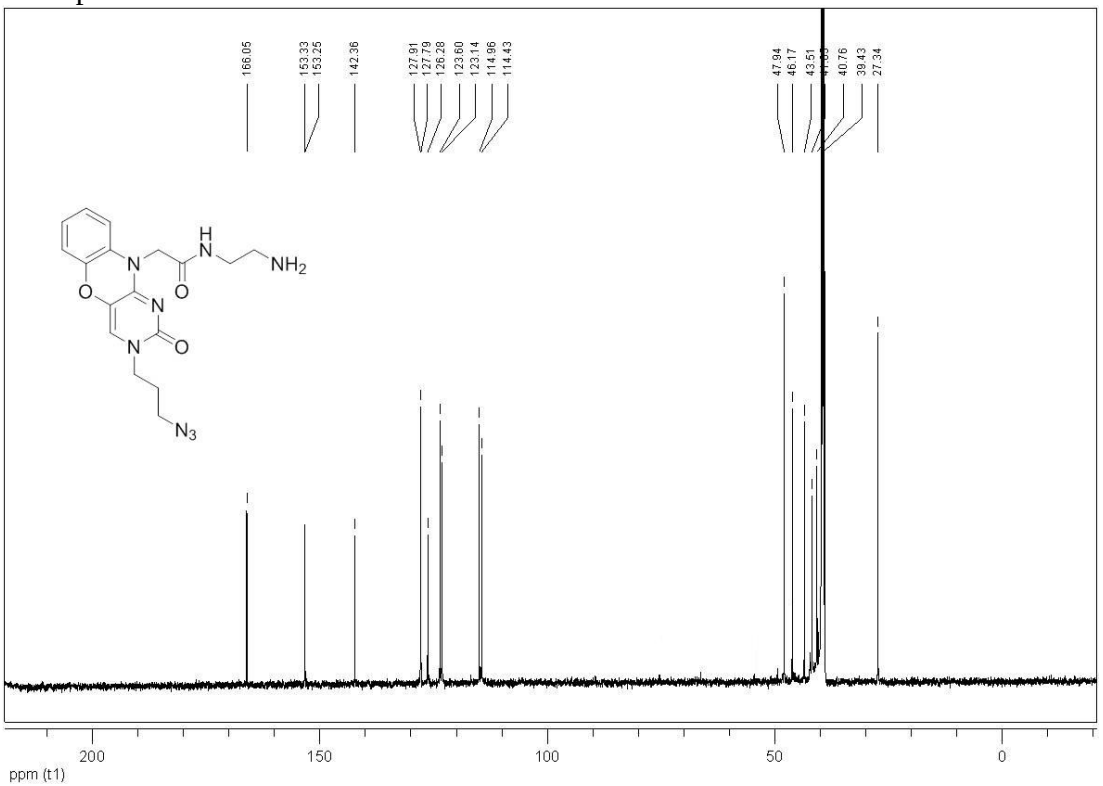

8-(3-aminopropoxy)-3-(3-aminopropyl)-1,3-diaza-2-oxophenoxazine **5**$^{\mathbf{pro}}$

1H spectrum

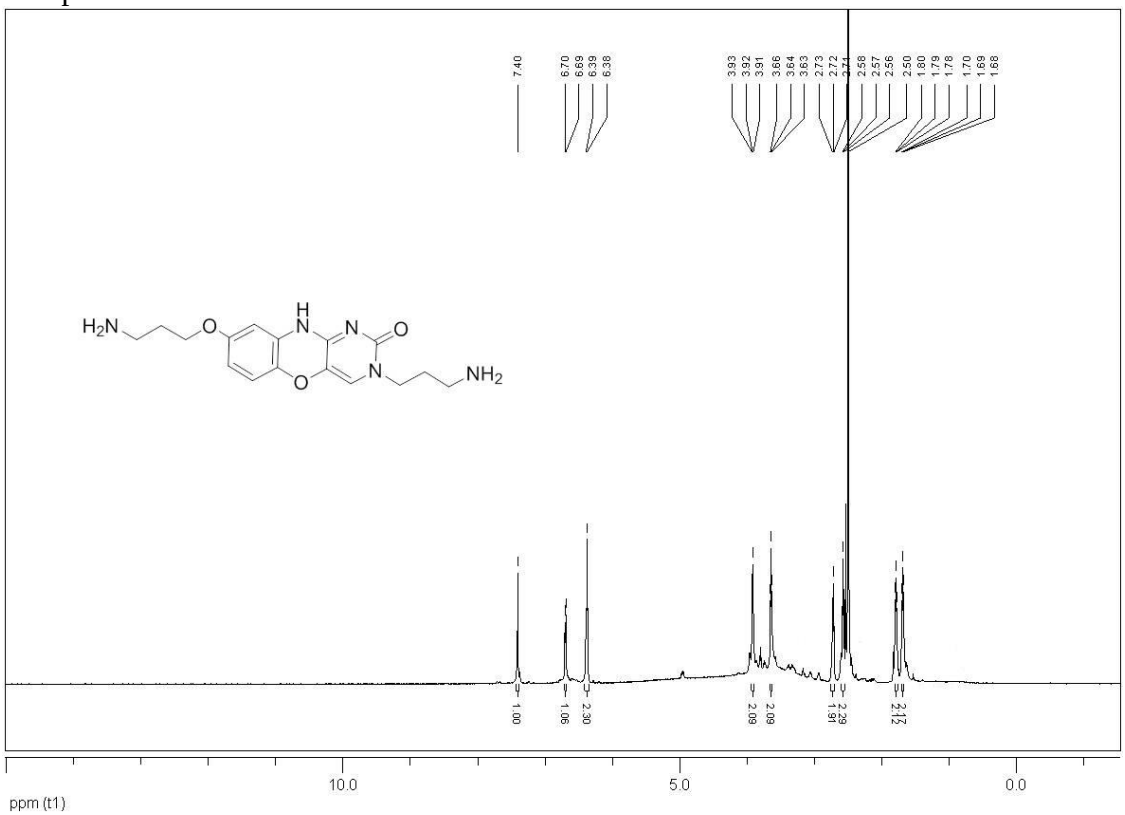

13C spectrum

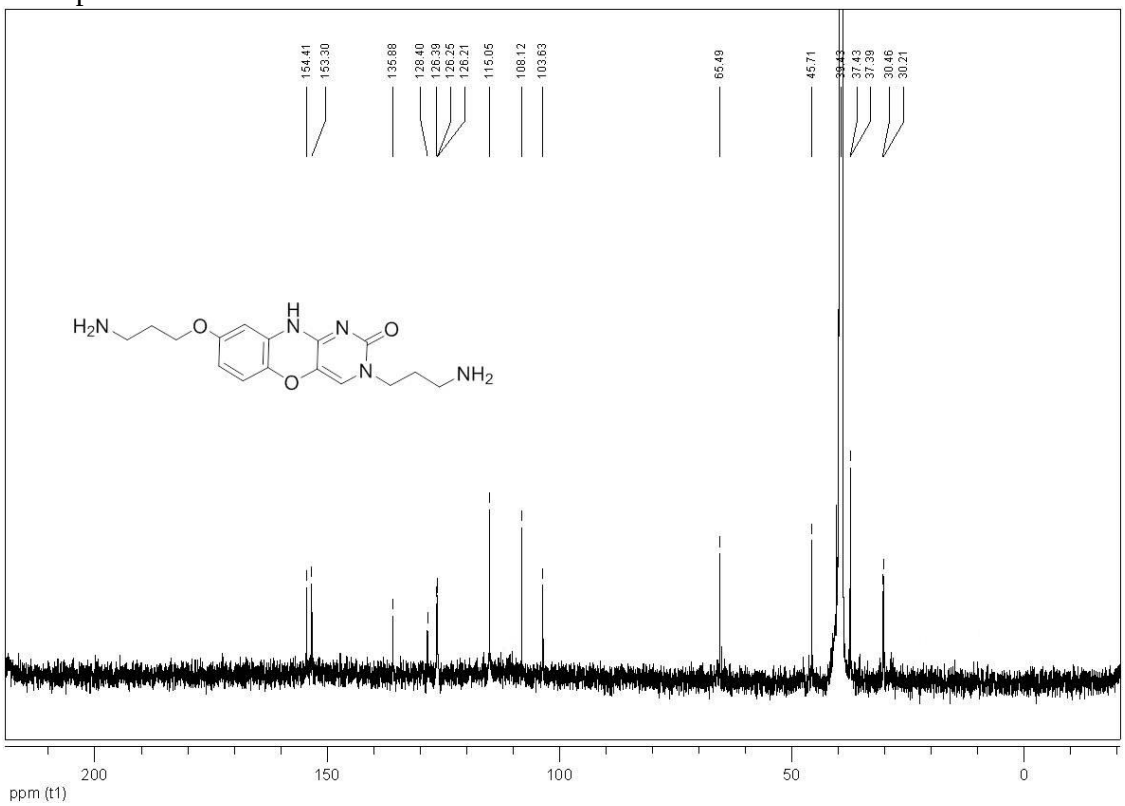

3-(3-aminopropyl)-1,3-diaza-2-oxophenoxazine **7**

1H spectrum

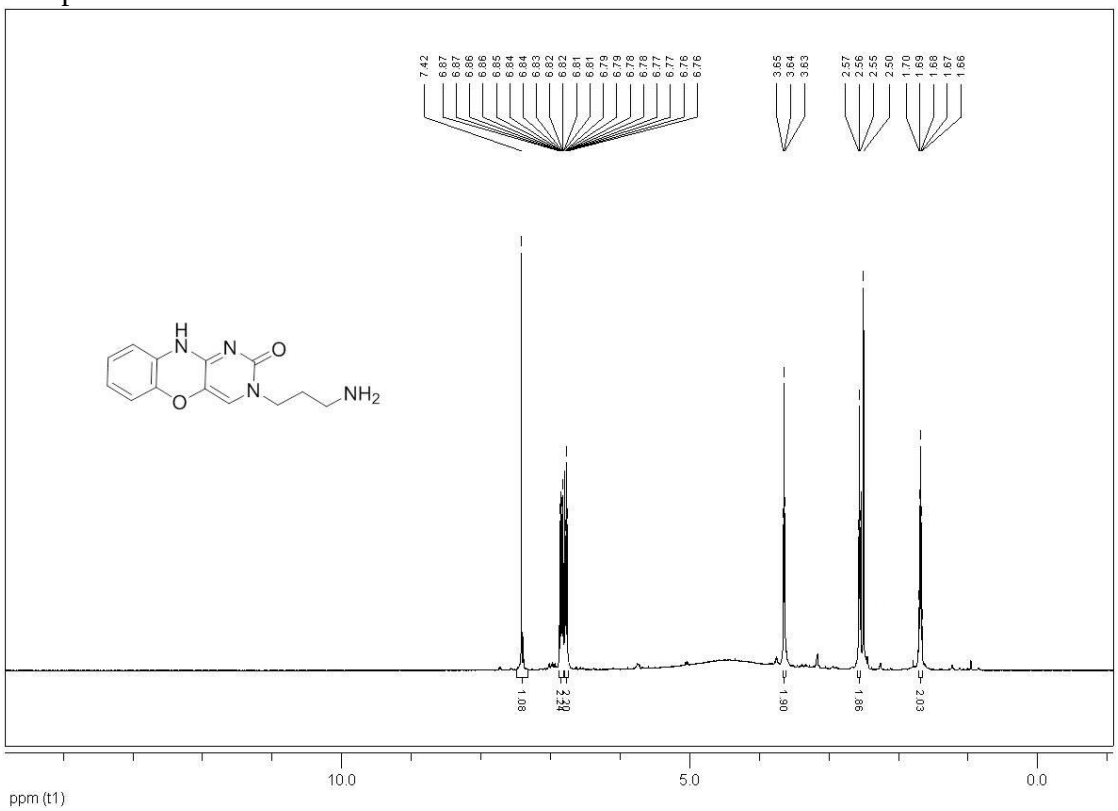

13C spectrum

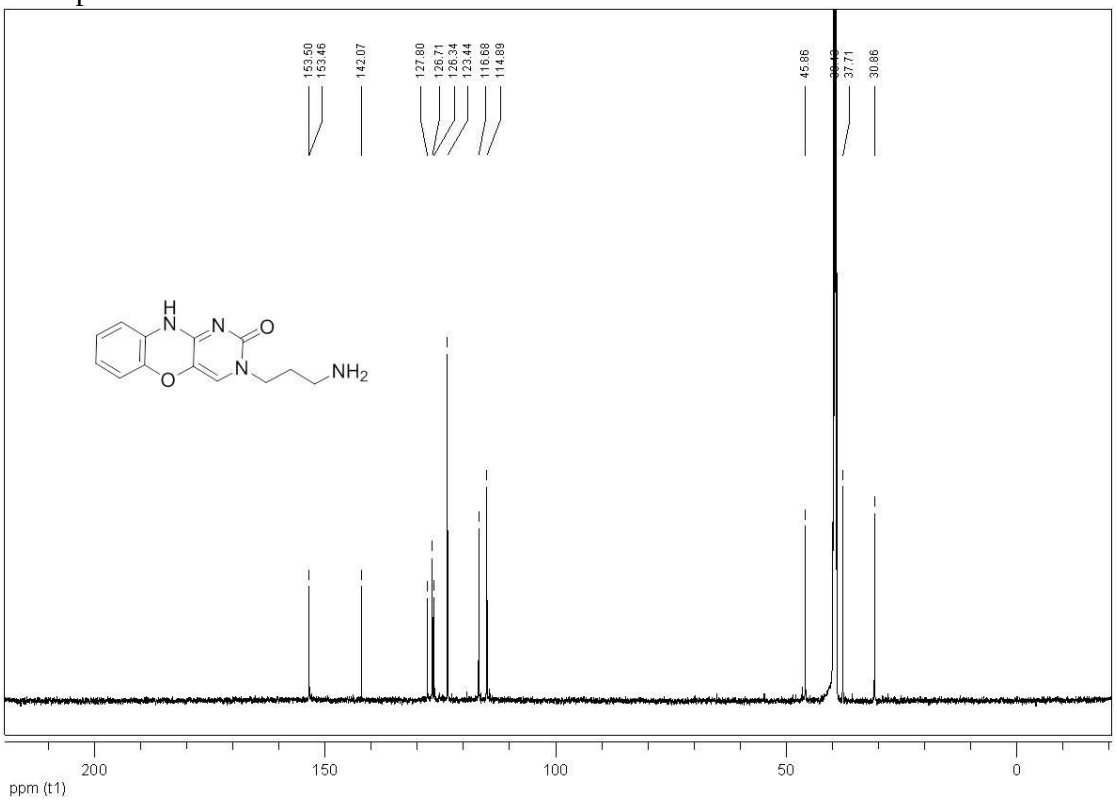

10-(2-((2-aminoethyl)amino)-2-oxoethyl)-3-(3-aminopropyl)-1,3-diaza-2-oxophenoxazine **9**

1H spectrum

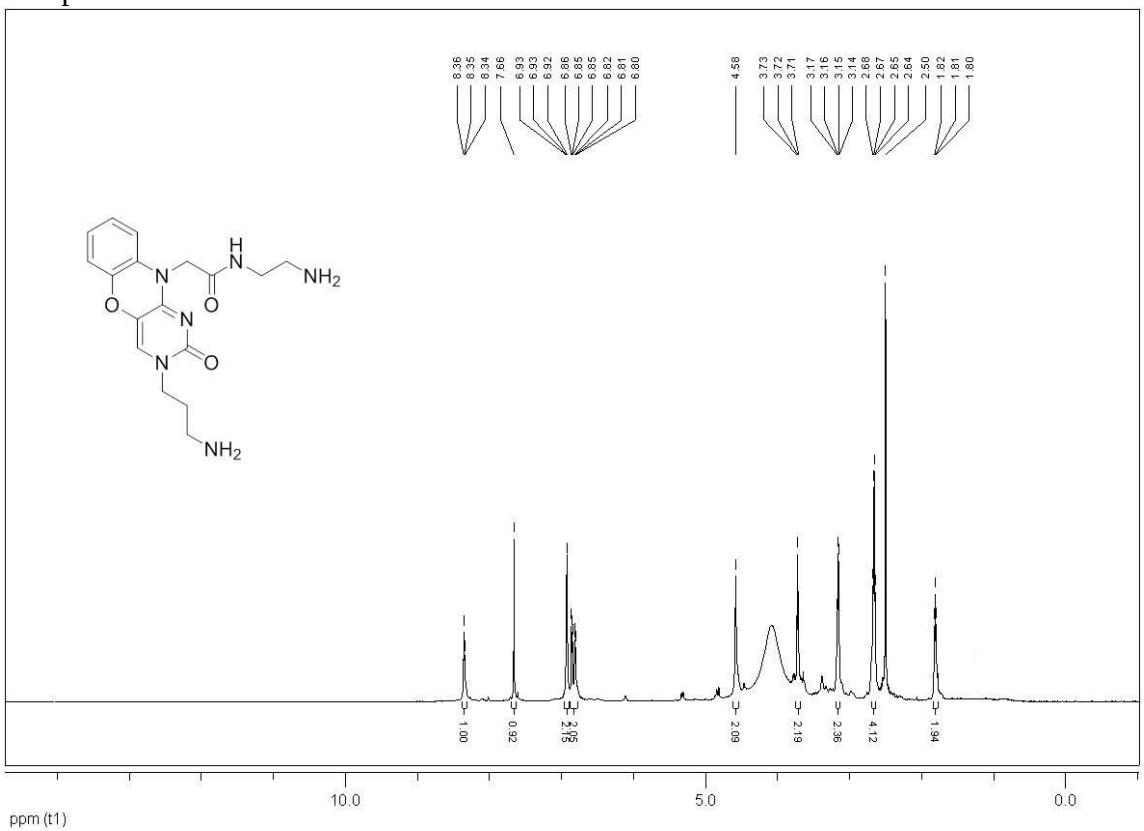

13C spectrum

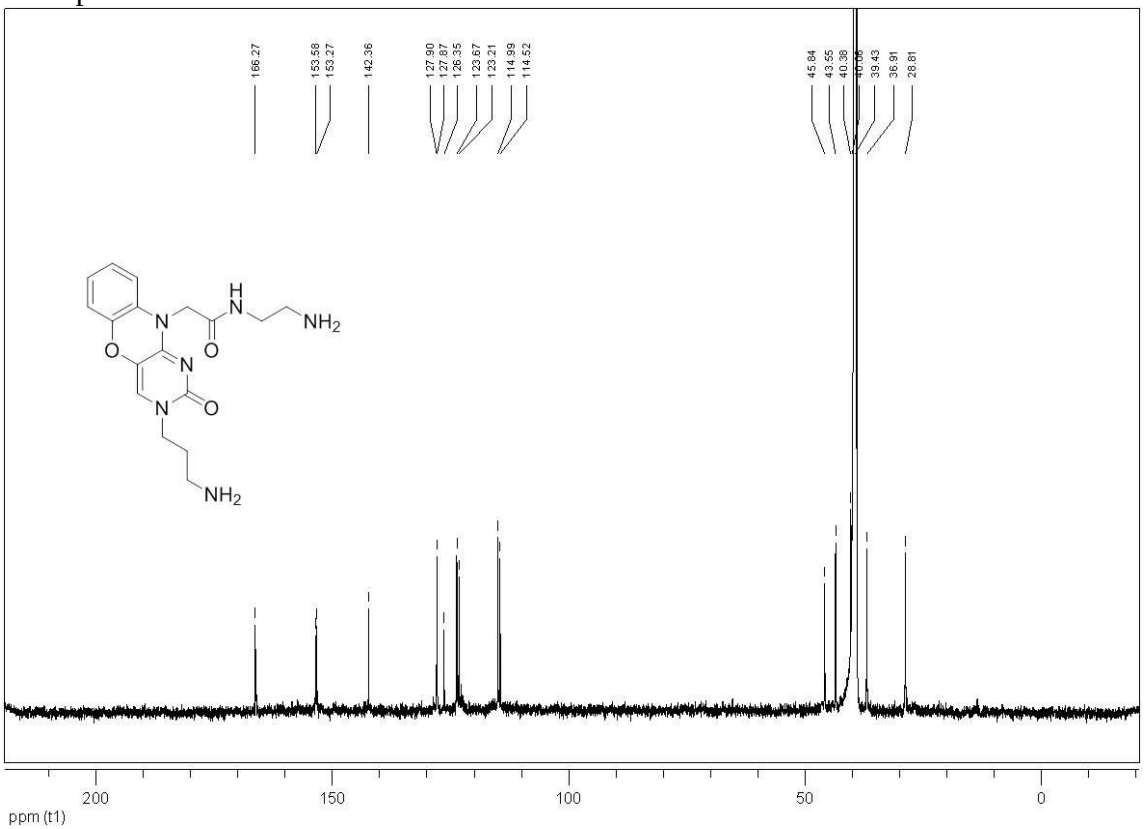

5. References

[1] a)R. Abagyan, M. Totrov, D. Kuznetsov, *Journal of Computational Chemistry* **1994**, *15*, 488; b) M. Totrov, R. Abagyan, *Proteins-Structure Function and Genetics* **1997**, 215.

[2] T. A. Halgren, *Journal of Computational Chemistry* **1996**, *17*, 490.

[3] J. Heyd, G. E. Scuseria, *Journal of Chemical Physics* **2004**, *121*, 1187.

[4] U. C. Singh, P. A. Kollman, *Journal of Computational Chemistry* **1984**, *5*, 129.

[5] C. I. Bayly, P. Cieplak, W. D. Cornell, P. A. Kollman, *Journal of Physical Chemistry* **1993**, *97*, 10269.

[6] M. J. Frisch, G. W. Trucks, H. B. Schlegel, G. E. Scuseria,M. A. Robb, J. R. Cheeseman, G. Scalmani, V. Barone,B. Mennucci, G. A. Petersson, H. Nakatsuji, M. Caricato,X. Li, H. P. Hratchian, A. F. Izmaylov, J. Bloino, G. Zheng,J. L. Sonnenberg, M. Hada, M. Ehara, K. Toyota, R. Fukuda,J. Hasegawa, M. Ishida, T. Nakajima, Y. Honda, O. Kitao,H. Nakai, T. Vreven, J. A. Montgomery Jr., J. E. Peralta,F. Ogliaro, M. Bearpark, J. J. Heyd, E. Brothers, K. N. Kudin,V. N. Staroverov, R. Kobayashi, J. Normand, K. Raghavachari, A. Rendell, J. C. Burant, S. S. Iyengar, J. Tomasi, M. Cossi, N. Rega, J. M. Millam, M. Klene, J. E. Knox, J. B. Cross, V. Bakken, C. Adamo, J. Jaramillo, R. Gomperts, R. E. Stratmann, O. Yazyev, A. J. Austin, R. Cammi, C. Pomelli, J. W. Ochterski, R. L. Martin, K. Morokuma, V. G. Zakrzewski, G. A. Voth, P. Salvador, J. J. Dannenberg, S. Dapprich, A. D. Daniels, O. Farkas, J. B. Foresman, J. V. Ortiz, J. Cioslowski and D. J. Fox, Gaussian 09, Revision A.1, Gaussian, Inc., allingford CT, 2009.

[7] Y. H. Dai, L. Z. Liao, D. Li, *Numerical Algorithms* **2004**, *35*, 249.

[8] Y. A. Arnautova, A. Jagielska, H. A. Scheraga, *Journal of Physical Chemistry B* **2006**, *110*, 5025.

[9] R. Abagyan, M. Totrov, *Journal of Molecular Biology* **1994**, *235*, 983.

[10] M. Totrov, R. Abagyan, *Proteins-Structure Function and Genetics* **1997**, 215.

[11] D.A. Case, I.Y. Ben-Shalom, S.R. Brozell, D.S. Cerutti, T.E. Cheatham, III, V.W.D. Cruzeiro, T.A. Darden, R.E. Duke, D. Ghoreishi, M.K. Gilson, H. Gohlke, A.W. Goetz, D. Greene, R Harris, N. Homeyer, Y. Huang, S. Izadi, A. Kovalenko, T. Kurtzman, T.S. Lee, S. LeGrand, P. Li, C. Lin, J. Liu, T. Luchko, R. Luo, D.J. Mermelstein, K.M. Merz, Y. Miao, G. Monard, C. Nguyen, H. Nguyen, I. Omelyan, A. Onufriev, F. Pan, R. Qi, D.R. Roe, A. Roitberg, C. Sagui, S. Schott-Verdugo, J. Shen, C.L. Simmerling, J. Smith, R. Salomon-Ferrer, J. Swails, R.C. Walker, J. Wang, H. Wei, R.M. Wolf, X. Wu, L. Xiao, D.M. York and P.A. Kollman (2018), AMBER 2018, University of California, San Francisco.

[12] S. Izadi, A. V. Onufriev, *Journal of Chemical Physics* **2016**, 145.

[13] a)M. Krepl, M. Zgarbova, P. Stadlbauer, M. Otyepka, P. Banas, J. Koca, T. E. Cheatham, P. Jurecka, J. Sponer, *Journal of Chemical Theory and Computation* **2012**, *8*, 2506; b)M. Zgarbova, F. J. Luque, J. Sponer, T. E. Cheatham, M. Otyepka, P. Jurecka, *Journal of Chemical Theory and Computation* **2013**, *9*, 2339; c)M. Zgarbova, J. Sponer, M. Otyepka, T. E. Cheatham, R. Galindo-Murillo, P. Jurecka, *Journal of Chemical Theory and Computation* **2015**, *11*, 5723.

[14] J. M. Wang, R. M. Wolf, J. W. Caldwell, P. A. Kollman, D. A. Case, *Journal of Computational Chemistry* **2004**, *25*, 1157.

[15] J. P. Ryckaert, G. Ciccotti, H. J. C. Berendsen, *Journal of Computational Physics* **1977**, *23*, 327.

[16] T. Darden, D. York, L. Pedersen, *Journal of Chemical Physics* **1993**, *98*, 10089.

[17] A. Onufriev, D. Bashford, D. A. Case, *Journal of Physical Chemistry B* **2000**, *104*, 3712.

[18] A. Singh, C. Biot, A. Viljoen, C. Dupont, L. Kremer, K. Kumar, V. Kumar, *Chemical Biology & Drug Design* **2017**, *89*, 856.

[19] V. B. Tsvetkov, T. S. Zatsepin, E. S. Belyaev, Y. I. Kostyukevich, G. V. Shpakovski, V. V. Podgorsky, G. E. Pozmogova, A. M. Varizhuk, A. V. Aralov, *Nucleic Acids Research* **2018**, *46*, 2751.